Mon. Not. R. Astron. Soc. **000**, 000–000 (0000) Printed 22 January 2022 (MN LaTeX style file v2.2)

Two-component outer ring and the Galactic spiral structure

A.M. Melnik[1⋆] and P. Rautiainen[2]
[1] *Sternberg Astronomical Institute, 13, Universitetskii pr., Moscow, 119992, Russia*
[2] *Astronomy Division, Department of Physics, University of Oulu, P.O. Box 3000, FI-90014 Oulun yliopisto, Finland*

arXiv:1108.3741v1 [astro-ph.GA] 18 Aug 2011

Accepted 2011 December 00. Received 2011 December 00; in original form 2011 December 00

ABSTRACT

Model of the Galaxy with the ring R_1R_2' can explain some large-scale morphological features of the Galactic spiral structure. The Carina-Sagittarius arm can consist of two ascending segments of the outer rings R_1 and R_2 which almost touch each other near the Carina region. The Perseus and Crux arms can be partially identified with the descending segments of the ring R_2. Model of the two-component outer ring can also explain the existence of some maxima in diagrams (l, V_{LSR}) which are supposed to correspond to the directions tangential to the spiral arms. On the basis of numerical simulations we propose two sketches of the ring structure of the Galaxy which include the bar, two outer rings, the inner ring, and the nuclear gas condensation, that may be a nuclear ring. Both sketches can explain the position of the Carina-Sagittarius arm with respect to the Sun.

Key words: Galaxy – spiral structure: Galaxy: kinematics and dynamics

1 INTRODUCTION

The best tracers of the Galactic spiral structure are HII regions – gas clouds ionized by young hot stars. Their radio emission penetrates the interstellar dust and they can be observed even in the distant parts of the Galactic disk. Heliocentric distances r for the faraway HII regions ($r > 6$) are usually determined from the kinematical models under the assumption that velocity deviations from the rotation curve are zero. The kinematic method yields an unambiguous distance for objects located outside the solar circle ($R > R_0$), but gives two possible distances corresponding to the same line-of-sight velocity inside the solar circle ($R < R_0$, where R – is the Galactocentric distance). The choice between "near" and "far" distances requires additional information, usually it is the data on the absorption/emission lines of HI/H_2CO or self-absorption in the HI line. The method is based on the analysis of velocities of the foreground clouds (Anderson & Bania 2009).

Georgelin & Georgelin (1976) using the distribution of 100 HII regions with the excitation parameter more than $U > 70$ pc cm^{-2} have proposed a 4-armed spiral pattern with the mean pitch angle of spiral arms of $i \approx 12°$. Their model can also explain the existence of so-called tangential directions – lines of sight corresponding to maxima in the thermal radio continuum, HI and CO emission – which are associated with the tangents to the spiral arms. These directions were first determined from the analysis of the longitude-velocity diagrams in HI (Kerr 1970; Burton & Shane 1970; Simonson 1970) which exhibited the distribution of gas temperature in coordinates (l, V_{LSR}) (l – the Galactic longitude, V_{LSR} – the heliocentric line-of-sight velocity V_r corrected for the solar motion to the apex) averaged over some range of Galactic latitudes b. The original model by Georgelin & Georgelin (1976) has been developed on the basis of new data (Lockman 1979; Downes et al. 1980; Caswell & Haynes 1987; Watson et al. 2003; Russeil 2003; Paladini et al. 2004; Russeil et al. 2007; Hou et al. 2009; Efremov 2011).

Russeil (2003) has grouped HII regions and molecular clouds into complexes of star formation which enables her to decrease the random errors in determination of mean velocities and kinematical distances. Locations of spiral arms supposed by Russeil (2003) practically coincide with those obtained by Georgelin & Georgelin (1976), though the spiral structure generally becomes more symmetrical. Russeil (2003) supposes that her sample of complexes including HII regions with high excitation parameter ($U > 60$ pc cm^{-2}) is complete all over the Galactic disk. For determination of kinematical distances she has used nearly flat rotation curve derived from objects with known photometric distances.

There are also other indicators of the Galactic spiral

⋆ E-mail: anna@sai.msu.ru

Table 1. Directions tangential to the spiral arms

N	longitude	Name	Other name
1	$l \sim 284°$	Carina arm	
2	$l \sim 310°$	Crux arm	Centaurus arm
3	$l \sim 327°$	Norma arm	Norma-3-kpc arm
4	$l \sim 339°$	3-kpc arm	start of Perseus arm
5	$l \sim 25, 31°$	Scutum arm	
6	$l \sim 51°$	Sagittarius arm	

structure. One of them is the giant clouds of molecular hydrogen (GMC) with the size of $\sim$ 40 pc and the mass of 10^4 – 10^6 $M_\odot$. Cohen et al. (1986) showed that GMCs outlined well the Carina arm. Dame et al. (1986) solved the ambiguity in the choice from the two kinematical distances in the first quadrant and selected objects of the Sagittarius arm. Grabelsky et al. (1988) compiled a catalogue of GMCs in the region $270 < l < 300°$ and identified the objects of the Carina arm. Also, the neutral hydrogen concentrates on the spiral arms (Oort et al. 1958; Kerr 1962) and is distributed quite non-uniformly outside the solar circle (Henderson et al. 1982; Kalberla et al. 2005; Levine et al. 2006).

We will show that two-component outer ring of class R_1R_2 can also explain many large-scale morphological features of the Galactic spiral structure. The paper has the following structure: Section 2 is devoted to tangential directions, the dynamical and kinematical aspects of the problem are discussed in Section 3, a brief description of dynamical models including the outer rings is given in Section 4, Section 5 presents results of a comparison of our models with observations.

2 TANGENTIAL DIRECTIONS AND THE NAMES OF THE SPIRAL ARMS

Englmaier & Gerhard (1999) and Vallée (2008) compiled information about directions tangential to the spiral arms. Generally, the tangential directions are connected with the existence of some intensity maxima in diagrams (l, V_{LSR}). Fig. 1 shows the distribution of ^{12}CO composed by Dame et al. (2001). The velocities of more than $\pm$150 km s^{-1} in the central region ($|l| \leqslant 10°$) can be explained by the presence of elliptical orbits in the central region. But, in general, gas at the positive longitudes, $10 < l < 90°$, has the positive velocities V_{LSR} while at negative longitudes, $-90 < l < -10°$, the negative ones. The extreme velocities at each direction are often called terminal velocities. Besides, the diagrams demonstrate the ridge-like intensity maxima that are often associated with the spiral arms. The directions where the "ridges" reach the curves of terminal velocities are thought as the tangential directions (Table 1).

Note also the presence of the bright emission at $l = 80°$ corresponding to the Cygnus region (l = 73–78°, r = 1.5 kpc) which is usually directly associated with the Local arm or spur (its another name is Orion-Cygnus arm) and is excluded from consideration.

The connection of bright spots in the diagrams (l, V_{LSR}) with a certain distance should be taken with great caution: in reality they can consist of a chain of clouds extended to several kpc along the line of sight (Adler & Roberts 1992). The problem is that the different models of the gas motion in the Galaxy can produce the very similar diagrams (l, V_{LSR}).

Fig. 2 illustrates the idea of tangential directions. It shows a regular spiral pattern with parameters: $i = 12.8°$, $r_0 = 2.1$ kpc, $\theta_0 = -20$, and $m = 4$ taken from the paper by Vallée (2008), as well as the tangential directions. It also exhibits and distribution of giant star-forming complexes from the catalogue by Russeil (2003). We can clearly see that every ray is tangent (or passes very close to the tangent) to the spiral arm. On the other hand, only the Carina arm is outlined well by star-forming complexes.

Note that the naming of the arms in literature is somewhat confusing: the Norma arm is sometimes called Norma-3-kpc arm, but the 3-kpc arm, in its turn, is also termed "start of Perseus arm" (see also Table 1). Another example is the Cygnus arm, which can easily be confused with the Cygnus region situated near the Sun (r = 1.5 kpc). This outer arm is also sometimes called "Perseus + I arm" or "Norma-Cygnus arm" (Vallée 2005, 2008).

There are no tangential directions to the outer Cygnus arm ($70 < l < 220°$, r = 5–9 kpc, R = 11–15 kpc), because it lies outside the solar circle. Interestingly, the Cygnus arm is absent on the schema supposed by Georgelin & Georgelin (1976). Its appearance is caused by two reasons: the principle of symmetry and discovery of new HII regions. Efremov (1998, 2011) identifies the HI superclouds outlining the Carina-Sagittarius arm and shows that the arm symmetrical to it doesn't coincide with the Perseus arm but lies beyond it. Additionally, Russeil (Russeil 2003; Russeil et al. 2007) discoveres many star-forming complexes in the region $70 < l < 220°$ at the distance range r = 4–10 kpc which cannot belong to the Perseus arm.

3 DYNAMICAL AND KINEMATICAL ASPECTS OF THE PROBLEM

Model suggested by Georgelin & Georgelin (1976) and developed in subsequent papers leaves open many questions. At the moment no N-body simulation with realistic rotation curve and the size of the bar can reproduce the classical 4-armed pattern. The main problem concerns the dynamical mechanism which could support the spiral pattern occupying a large part of the galactic disk (see surveys by Toomre 1977; Athanassoula 1984; Binney & Tremaine 2008).

The concept of the density-wave theory (Lin & Shu 1964; Bertin & Lin 1996) where the spiral arms are forming at places of crowding of the orbits deserves special attention. A lot of researches think that at least two major spiral arms in the Galaxy are the density-wave spiral arms. But density-waves create specific distribution of velocities in the young disk population that is forming due to adjustment of epicyclic motions of stars in accordance with orbital rotation (Lin et al. 1969). Kalnajs (1973) suggests to consider stellar orbits in the reference frame co-rotating with the speed of the spiral pattern Ω_p, in which the orbits are looking as

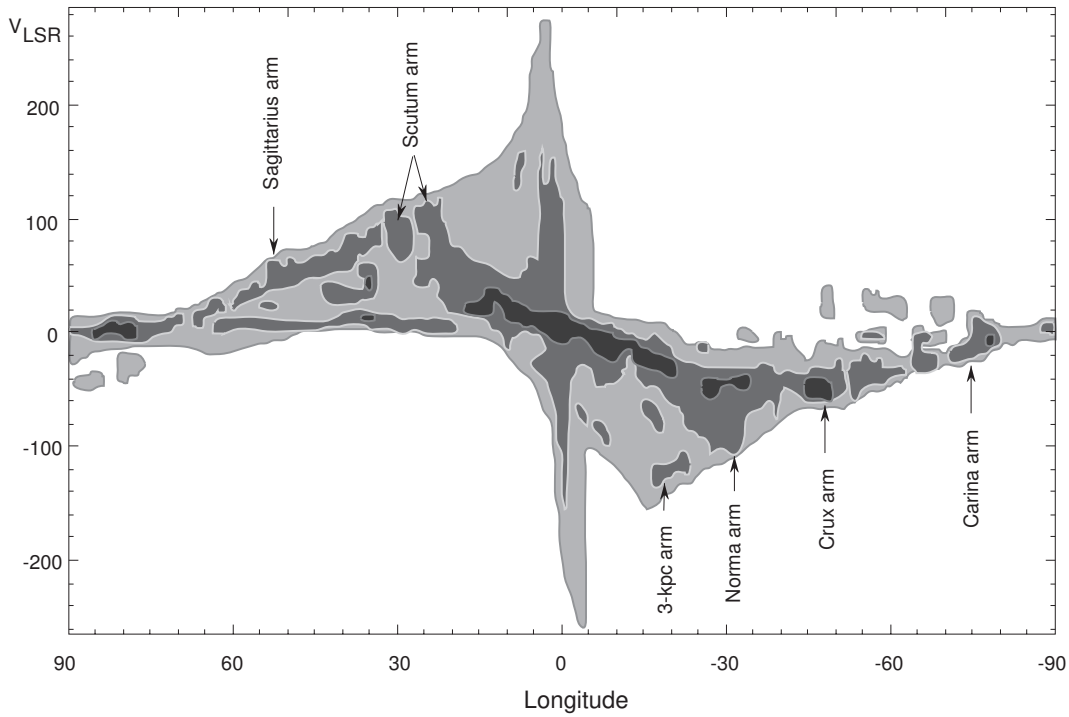

Figure 1. Sketch of the diagram (l,V_{LSR}) of the ^{12}CO distribution (Dame et al. 2001). The emission is averaged in the range $b = \pm 2°$. It also indicates the positions of maxima corresponding to the directions tangential to the spiral arms.

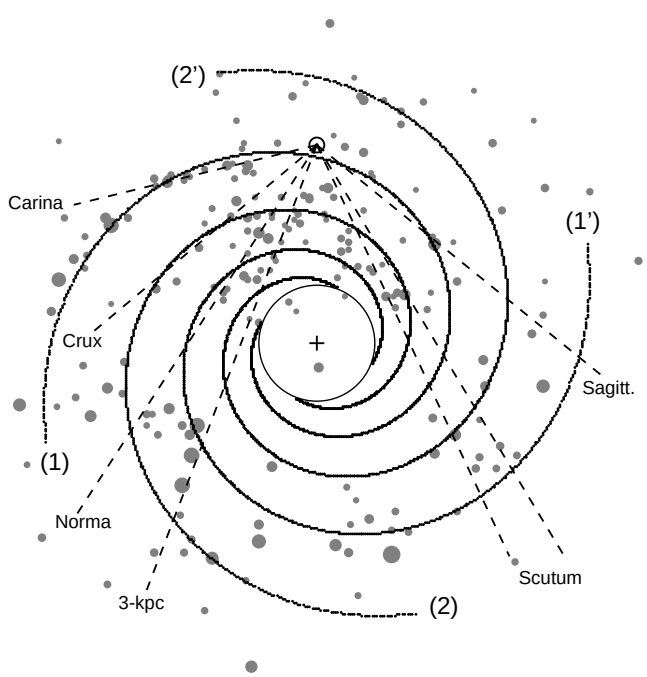

Figure 2. Regular spiral pattern with parameters of logarithmic spirals: $i = 12.8°$, $r_0 = 2.1$ kpc, $\theta_0 = -20°$, and $m = 4$ (Vallée 2008). 1: Sagittarius-Carina arm, 2: Scutum-Crux arm, 1′: Norma-Cygnus arm, and 2′: Perseus arm. It also shows the tangential directions to the spiral arms. Giant star-forming complexes ($U > 60$ pc cm^{-2}) from the catalogue by Russeil et al. (2007) are depicted by grey circles whose size is proportional to the excitation parameter.

pure ellipses or ellipses with the "dimples". If we know the direction of rotation of disk stars in the adopted frame then we can divide their orbital ellipses into the ascending and descending segments, where stars go away ($V_R > 0$) and toward ($V_R < 0$) the Galactic center, respectively. Fig. 3 illustrates the idea that orbit crowding occurs at the descending or ascending segments of ellipses, and the choice between them depends on the sense of orbital rotation. This must be viewed in the reference frame rotating with the speed Ω_p in which the sense of rotation is determined by the position of the corotation radius (CR) with respect to the region considered. Thus, the knowledge of the direction of radial component V_R of velocities in the spiral arms allows us to restrict the region where the CR can be located and thereby roughly estimate the value of the angular speed of the spiral pattern Ω_p.

The study of the kinematics of young stars in the regions of intense star formation yields unexpected distribution of the velocities. The radial component V_R of the velocity in the Carina, Cygnus, and Perseus regions is directed toward the Galactic center ($V_R < 0$) while it is directed away from it ($V_R > 0$) in the Sagittarius region and in the Local System (Mel'nik et al. 1999, 2001; Mel'nik 2003; Sitnik 2003; Mel'nik & Dambis 2009). This means that the Perseus and Sagittarius regions cannot be parts of the same density-wave spiral pattern rotating with one pattern speed. Note that two-armed model of the Galactic spiral structure with the angular speed of $\Omega_p = 13.5$ km s^{-1} kpc^{-1} (Lin et al. 1969) can reproduce well the kinematics in the Perseus region (Roberts 1972; Burton & Bania 1974; Humphreys 1976, and other papers). But the kinematics of the Sagittarius region indicates that it must be located outside the CR and

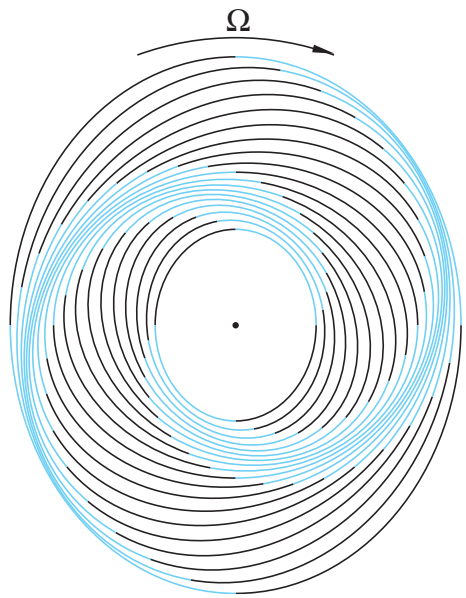

Figure 3. Segments of stellar orbits with the negative and positive radial velocity V_R in the trailing density-wave spiral arms located inside the CR. The galaxy rotates clockwise. Motions are considered in the reference frame co-rotating with the spiral pattern, in which stars also rotate clockwise. The ascending segments of ellipses ($V_R > 0$) are shown in black whereas the descending ones ($V_R < 0$) are shown in blue. Inside the CR the crowding of the orbits occurs on the descending segments of ellipses.

rotates with the speed of more than $\Omega_p > 38$ km s^{-1} kpc^{-1} (Mel'nik 2006).

There are a lot of evidences that our Galaxy includes the bar. The estimation of the length of the bar has increased from initial $R_{bar} = 2 - 3$ kpc (Blitz & Spergel 1991; Binney et al. 1991; Blitz et al. 1993) to the current values $R_{bar} = 3 - 5$ kpc (Benjamin et al. 2005; Babusiaux & Gilmore 2005; Habing et al. 2006; Cabrera-Lavers et al. 2007; Pohl et al. 2008; Gerhard 2011). Dynamical models of the gaseous medium moving in the Galactic potential perturbed by the bar reproduce the so-called "parallelograms" on the diagrams (l, V_{LSR}) in the central region (Weiner & Sellwood 1999; Fux 1999; Englmaier & Gerhard 1999, 2006). The general consensus is that the major axis of the bar is oriented in the direction $\theta_b = 15$–$45°$ in such a way that the end of the bar closest to the Sun lies in the first quadrant.

The concept that the Galaxy can include several modes rotating with different angular speeds was actively developed in the beginning of the 2000s. The rapidly rotating bar ($\Omega_b = 40$–60 km s^{-1} kpc^{-1}) and the slower mode ($\Omega_{sp} = 20$–40 km s^{-1} kpc^{-1}) could explain the gas kinematics in the central region and at larger distances, respectively (Bissantz & Gerhard 2002; Bissantz et al. 2003). However, application of a two-mode model to the Galaxy appears to be much harder than expected. On the one hand, there are many dynamical models, where the disk forms a pattern rotating slower than the bar (Sellwood & Sparke 1988; Masset & Tagger 1997; Rautiainen & Salo 1999, 2000). On the other hand, after introducing physical units the strongest slow mode turns to have the pattern speed of $\Omega_{sp} \approx 30$ km s^{-1} kpc^{-1}, which is too high to explain the kinematics of young stars in the Perseus region.

In parallel with the concept of modes a different approach has been developed. Here the spiral arms are regarded as a subsequent generation of short-lived spiral perturbations connected with each other through the resonances: the CR of each next wave is located at one of the resonances of the previous one (Sellwood & Lin 1989; Sellwood & Kahn 1991; Sellwood 2000, 2011). Nevertheless, it is questionable whether this approach can explain the existence of long spiral arms similar to the Carina one in the Galaxy (Fig. 2).

4 MODELS OF THE GALAXY INCLUDING THE OUTER RING

The essential characteristic of the galaxies with the outer rings and pseudorings – incomplete rings made up of spiral arms – is the presence of the bar (Buta 1995; Buta & Combes 1996). Since the outer rings have an elliptic form, the broken outer rings (pseudorings) resemble two tightly wound spiral arms. Two main classes of the outer rings and pseudorings have been identified: the R_1 rings (R_1' pseudorings) elongated perpendicular to the bar and the R_2 rings (R_2' pseudorings) elongated parallel to the bar. In addition, there is a combined morphological type R_1R_2' which shows elements of both classes. The R_2 rings have elliptical shape, but the R_1 rings are often "dimpled" near the bar ends (Buta 1995; Buta & Crocker 1991).

The test particle simulations (Schwarz 1981; Byrd et al. 1994; Rautiainen & Salo 1999) and N-body simulations (Rautiainen & Salo 2000) show that the outer rings are typically located in the region of the Outer Lindblad Resonance (OLR). Schwarz (1981) connected two main types of the outer rings with two main families of periodic orbits existing near the OLR of the bar (Contopoulos & Papayannopoulos 1980; Contopoulos & Grosbol 1989). The stability of orbits enables gas clouds to follow them for a long time period. The R_1-rings are supported by $x_1(2)$-orbits (using the nomenclature of Contopoulos & Grosbol 1989) lying inside the OLR and elongated perpendicular to the bar, while the R_2-rings are supported by $x_1(1)$-orbits situated a bit outside the OLR and elongated along the bar.

The bar semi-major axis in the Galaxy is supposed to lie in the range $a = 3$–5 kpc. For the flat rotation curve and a fast rotating bar this means that the bar angular speed Ω_b is limited by the interval $\Omega_b = 40$–70 km s^{-1} kpc^{-1} and the OLR of the bar is located in the solar vicinity: $|R_{OLR} - R_0| < 1.5$ kpc. The studies of the kinematics of old disk stars in a small solar vicinity, $r < 250$ pc, revealed a bimodality in the distribution of (u, v) velocities which was also interpreted as a result of the solar location near the OLR of the bar (Kalnajs 1991; Dehnen 2000; Fux 2001; Chakrabarty 2007; Minchev et al. 2010, and other papers). Thus, the presence of an outer ring in the Galaxy is a plausible possibility to be considered.

In addition to the outer rings, the Galaxy can include an inner ring or pseudoring surrounding the bar which manifests itself in the so-called 3-kpc arm(s) (Fux 1999; Dame & Thaddeus 2008; Churchwell et al. 2009). Also, a hypothesis about the presence of a nuclear

ring with a major axis of $\sim$ 1 kpc is considered (Rodriguez-Fernandez & Combes 2008).

With using the simulation code developed by H. Salo (Salo 1991; Salo & Laurikainen 2000) we have constructed two different types of models (models with analytical bars and N-body simulations) which reproduce the kinematics of OB-associations in the Perseus and Sagittarius regions. The kinematics of young stars in the Perseus region indicates the existence of the R_2 ring while the velocities in the Sagittarius region suggest the presence of the R_1 ring in the Galaxy. Our models have nearly flat rotation curves. The major and minor axes of the bar have the values of $a = 4.0$ and $b = 1.2$ kpc. The value of the solar position angle θ_b providing the best agreement between the model and observed velocities is $\theta_b = 45 \pm 5^\circ$. The bar angular speed lies in the range $\Omega_b = 42$–55 km s^{-1} kpc^{-1} (Mel'nik & Rautiainen 2009; Rautiainen & Mel'nik 2010, hereafter Papers I and II, respectively).

In the present paper we use the distribution of OB-particles in model No. 3 obtained in series of models with analytical bars for the time moment $T = 15$ ($\sim$ 1 Gyr). Model 3 was chosen due to presence of the inner ring which still persists by $T = 1$ Gyr. As for the outer rings, all models considered produce the similar distribution of OB-particles on the galactic periphery (Paper I). We also use the distribution of gas and stellar particles in N-body model averaged for the time interval $T = 5$–6 Gyr. The averaging over large time interval reduces the influence of slow modes and occasional perturbations (Paper II).

5 RESULTS

5.1 Ring R_1R_2' and the distribution of giant star-forming complexes

In this section we will use data from the catalogue by Russeil et al. (2007), particularly, the sample of giant star-forming complexes with the excitation parameter of more than $U > 60$ pc cm^{-2} that includes 194 regions in the range of Galactocentric distances $0 < R < 12$ kpc, 76% of them have only kinematical distances.

The distance scale in our models (Papers I and II) is adjusted to the so-called short distance scale of classical Cepheids (Berdnikov et al. 2000). Distance scale for star-forming complexes from the catalogue by Russeil et al. (2007) r_0 is close to that for OB-associations (Humphreys & McElroy 1984; Blaha & Humphreys 1989), so to match it with the short distance scale, we used the same scaling factor of $f = 0.8$ ($r = fr_0$), which was used for reducing the distance scale for OB-associations (Sitnik & Mel'nik 1996; Dambis et al. 2001; Mel'nik & Dambis 2009).

Fig. 4 exhibits the distribution of giant star-forming complexes and that of OB-particles from the series of models with analytical bars (Paper I). It also demonstrates the position of the regions of intense star-formation studied in Papers I and II. The Sagittarius region ($x = 0.5$, $y = 6.0$ kpc) lies on the segment of the ring R_1, whereas the Carina region ($x = -1.5$, $y = 6.5$ kpc) occupies the intermediate position between two outer rings in the place where they come closest to each other. The Perseus region ($x = 2.0$, $y = 8.0$ kpc) and the Local System ($x = 0.0$, $y = 7.4$ kpc) belong to the ring R_2, while the Cygnus region ($x = 1.5$, $y = 6.9$ kpc) appears to lie in the inter-ring space. The Galactocentric distance of the Sun is adopted to be $R_0 = 7.1$ (Rastorguev et al. 1994; Dambis et al. 1995; Glushkova et al. 1998).

Outer rings can be divided onto the ascending ($V_R > 0$) and descending ($V_R < 0$) segments. On the ascending segments (segments C-D-E and 5-6-7 in fig. 6 of Paper I), the Galactocentric distance R decreases with the increase of the azimuthal angle θ. This becomes clear if we remember that the closed orbits emerge only in the reference frame co-rotating with the bar. The outer rings lie near the OLR of the bar where disk objects rotate slower than the bar, therefore, in the reference frame co-rotating with it they will move in the direction opposite that of the Galactic rotation, i.e. counterclockwise. On the descending segments of the outer rings (segments 3-4-5 and E-F-G in fig. 6 of Paper I) the Galactocentric distance R increases with the increase of θ. Note also that ascending segments of the outer rings can be regarded as fragments of the trailing spiral arms while the descending ones – as those of the leading spiral arms.

The Carina arm is often regarded as the major spiral arm in the Galaxy. It begins near the Carina region and unwinds counterclockwise along the Galactocentric angle at $|\Delta\theta| \approx 90^\circ$. It is evident that the star-forming complexes related to the Carina arm fall nicely on the ascending segment of the ring R_2: the deviation doesn't exceed 15% of the heliocentric distance r. Note also that the objects related to the Sagittarius arm are situated near the ascending segment of the ring R_1. Although most of the researchers consider the Carina-Sagittarius arm as a single spiral arm, it could consist of two ascending segments of the outer rings R_1 and R_2 which almost touch each other near the Carina region ($x = -1.5$, $y = 6.5$ kpc). It is difficult to say anything about another pair of the ascending segments of the outer rings, but it is possible that they can be identified with the Norma-Cygnus arm symmetrical to the Carina-Sagittarius one. If the ascending segments of the outer rings were much brighter than the descending ones, then the Galactic spiral structure would be considered as 2-armed. In this context the 4-armed pattern suggests a significant brightness of the descending segments. The Perseus and Crux arms can be partially identified with the descending segments of the ring R_2. Interestingly, the giant complex 475 ($l = 352.8^\circ$, $b = 1.3^\circ$) (Russeil et al. 2007), which is the brightest in the Crux arm and practically determines its position, falls exactly on the descending segment of the ring R_2 (see its location in Fig. 8a).

We also studied the position of the outer rings with respect to the tangential directions. It turned out that model of the two-component outer ring can also explain the appearance of some of them: the line of sight in the direction of $l = 284^\circ$ is almost tangential to the outer ring R_2, and the rays in the directions of $l = 310^\circ$ and of 51° are tangents to the ring R_1 (Fig. 4). In addition, the lines of sight in the range of $l = 25$–31° are pointed to the end of the bar closest to the Sun. However, the directions of $l = 327^\circ$ and of 339° cannot be identified with any tangents to the rings or to the bar.

Fig. 4 also exhibits the gas-density distribution in N-body model (Paper II). As was expected, the line of sight in the directions of $l = 284^\circ$ (Carina arm) and of 51° (Sagittarius arm) cross a huge gas column at their way through

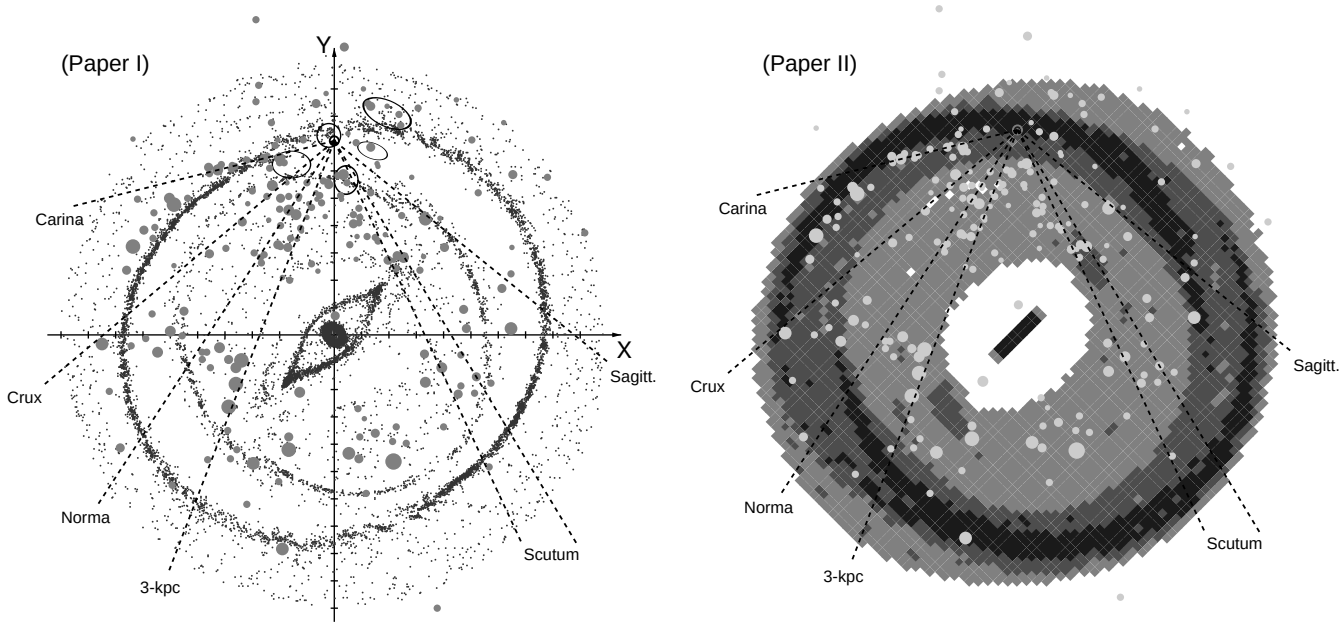

Figure 4. Comparison of the distribution of model particles with the distribution of giant star-forming complexes (Russeil et al. 2007). Left panel: distribution of OB-particles (black points) in model with analytical bar (Paper I). It also indicates the boundaries of the regions of intense star formation studied in Papers I and II. A division on the X and Y axis corresponds to 1 kpc. Right panel: gas-density distribution in N-body model averaged in small squares (Paper II). The light-gray, dark-gray and black colors represent squares containing the increasing number of particles. Giant complexes ($U > 60$ pc cm^{-2}) are depicted as circles whose size is proportional to the excitation parameter U. The tangential directions to the spiral arms are also shown (Table 1). The adopted value for the solar position angle with respect to the bar is $\theta_b = 45°$. The Galaxy rotates clockwise.

the combined R_1R_2 outer ring. The rays in the direction of $l = 25$–$31°$ intersect a region of high gas content located near the end of the bar. In distinction from models with analytical bars, N-body model retains a lot of gas near the bar ends.

5.2 Ring R_1R_2' and the diagrams (l, V_{LSR})

We assume that the variations in the ^{12}CO antenna temperature are caused by variations in the number of small unresolved molecular cloudlets falling within the field of the telescope (Mihalas & Binney 1981). If we associate these small clouds with gas particles in our models then the most bright regions in the observational maps must correspond to the regions of high column density in the model diagrams.

Fig. 5 shows the distribution of gas particles in the plane (l, V_{LSR}) built for model with analytical bar (Paper I) and for N-body simulation (Paper II). It also indicates the positions of the observational maxima near the terminal velocity curves which are supposed to correspond to the directions tangential to the spiral arms. It is seen that the model diagrams reproduce the intensity maxima in the direction of the Carina, Crux, Norma, and Sagittarius arms. Moreover, N-body model also creates the maxima in the directions of the Scutum and 3-kpc arms. Our models also produce the velocity peak of more than $|V_{LSR}| > 150$ km s^{-1} in the central region, $-5 < l < 5°$.

Fig. 6 demonstrates the distribution of model particles in the Galactic plane (Paper I) and their positions in the diagram (l, V_{LSR}). The Galactic plane is divided into annuli. The fan-shaped structure of the diagram is obvious: particles located at different annuli occupy different strip-like zones in the diagram. The larger the radius of the annulus the larger the angle between the corresponding strip and the vertical axis. Interestingly, the central peak is forming not only by objects of the nuclear ring but also by particles of the inner ring.

Note that our model diagrams (l, V_{LSR}) don't reproduce the so-called "Molecular Ring" on the observed CO-survey (Fig. 1) – the ridge of enhanced emission that extends from the Scutum tangential point to the Norma one (Dame et al. 2001). This observational feature is sometimes interpreted as a molecular ring (Binney et al. 1991) or as spiral arms emanating from the bar (Fux 1999). In any case our models need some modification to keep more gas near the bar ends.

5.3 Ring model of the Galaxy

Let us consider a new model of the Galaxy that includes two outer rings, the inner ring, and the nuclear ring. Fig. 7 represents the basic sketch of the galactic ring structure composed on the base of sketches designed by Buta (1986). The resonance rings are supported by the periodic orbits which are elongated parallel or perpendicular to the bar and change their orientation near the OLR, CR, and ILR(s), some chaotic orbits also share similar characteristics (Contopoulos & Papayannopoulos 1980; Contopoulos & Grosbol 1989). But not only resonant processes determine the formation of ring-like structures in the galactic disks. They are also affected by the gas flow outwards or inwards due to torque from the bar. The central region often includes the inner spiral arms that connect La-

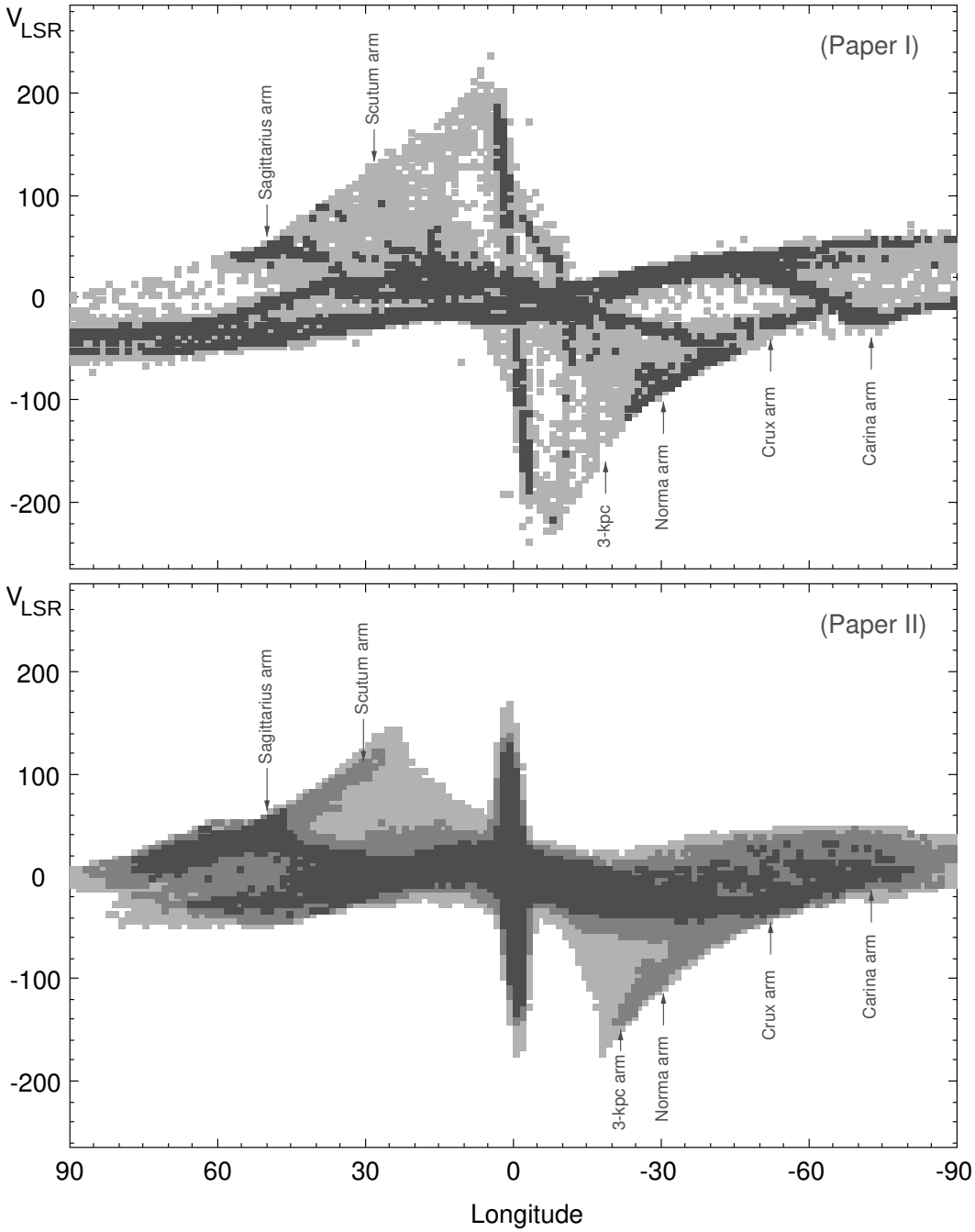

Figure 5. Diagrams (l, V_{LSR}) built for model with analytical bar (Paper I) and for N-body simulation (Paper II). The darker colors correspond to the cells with increasing number of particles n. In the upper panel two gray tones represent cells with n below and above the average value $\overline{n}$ ($\overline{n} = 11$). In the lower panel three gray tones show the cells with $10 < n < \overline{n}$, $\overline{n} < n < 2\overline{n}$, and $n > 2\overline{n}$ ($\overline{n} = 427$). It also indicates the maxima connected with the directions tangential to the spiral arms.

grangian points L_1 and L_2 with the nuclear ring or with the galactic center, which are shocks caused by the bar (Athanassoula 1992). Note also that outer rings R_1 and R_2 in the basic sketch connect with each other, but such connection is sometimes absent in numerical simulations and in images of real galaxies (for example, NGC 1211). The connection between the inner ring and the outer ring R_1 can be missing as well (for example, NGC 3081, Buta et al. 2007)

The application of the basic ring structure to the Galaxy doesn't give an unambiguous picture. On the basis of numerical simulations we designed two sketches of the Galactic spiral structure (Fig. 8). In sketch A we try to reproduce the distribution of gas particles in model with analytical bar (Paper I) while in sketch B – the distribution of gas and star particles in N-body simulation (Paper II). Both sketches have many similar features: the bar is represented as an gray ellipse with the semi-axes $a = 4.0$ and $b = 1.2$ kpc, the position angle of the Sun with respect to the bar equals $\theta_b = 45°$, the outer ring R_2 is approximated by an ellipse elongated along the bar with the semi-axes $a_2 = 8.0$

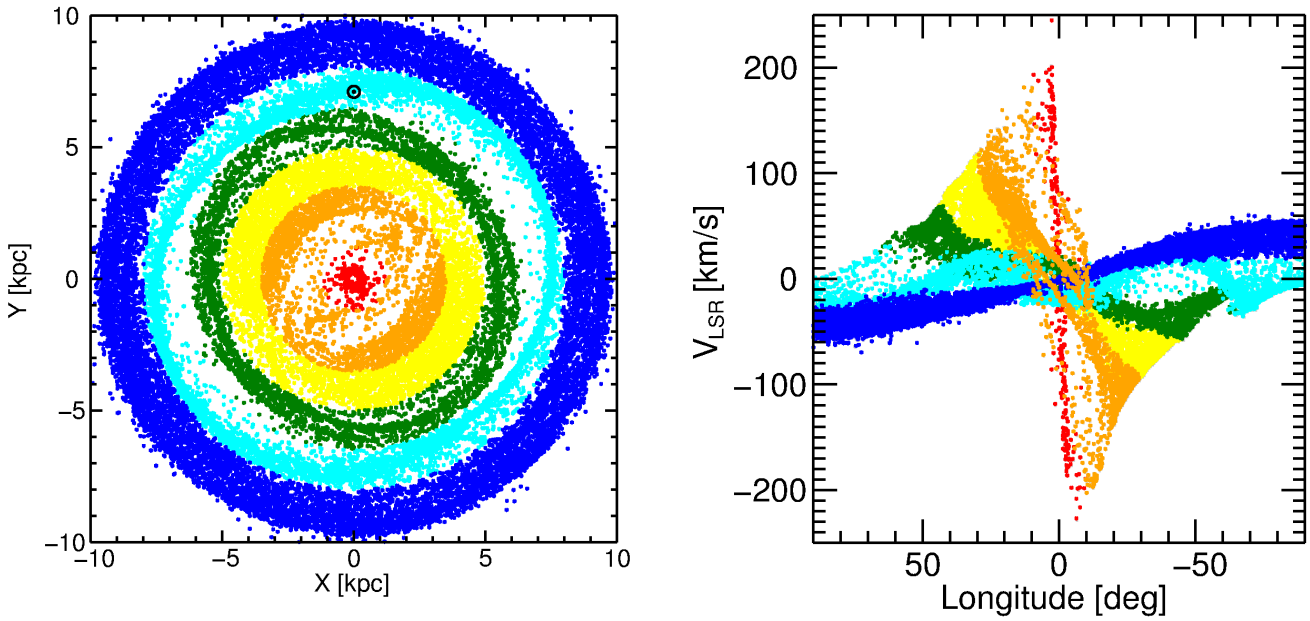

Figure 6. Left panel: the distribution of gas particles in the Galactic plane in model with analytical bar (Paper I). The size of the frame is 20 kpc. Particles located in different annuli are shown in different gray tones. Right panel: the position of particles selected in the diagram (l, V_{LSR}). The diagram has fan-shaped structure: objects of different annuli are located in strip-like zones turned at different angles to the vertical axis. The larger the annulus, the greater the angle between the corresponding strip and the vertical axis.

and $b_2 = 7.2$ kpc, which is in good agreement with the distribution of OB-particles in models with analytical bars (Paper I). The main differences of the sketches A and B lie in the size of the ring R_1, in the shape of the inner ring, and in the orientation of the central gas condensation.

In sketch A the CR of the bar lies at $R = 4.0$ kpc – just at the bar ends. The R_1 ring reaches only the radius of $R = 6.0$ kpc thereby forming a gap between the two outer rings. The inner structure is represented by the pointed inner ring connecting the bar ends with the nuclear ring. The connection between the inner ring and the outer ring R_1 is also absent. The nuclear ring in represented by an ellipse elongated perpendicular to the bar with the semi-axes $a_n = 0.8$ and $b_n = 0.6$ kpc.

In sketch B the CR of the bar is located at $R = 4.6$ kpc. The R_1 ring begins near the CR and reaches for the OLR of the bar so that there is no gap between the rings R_1 and R_2. In N-body simulation the ring R_1 is forming mainly in stellar population. The gaseous inner ring has more round shape here compared with sketch A. The central gas condensation is represented by an ellipse elongated along the bar with semi-axes $a_n = 0.8$ and $b_n = 0.2$ kpc.

Both sketches can easily explain the location of the Sagittarius-Carina arm with respect to the Sun. This arm can consist of two ascending segments of the outer rings R_1 and R_2. At the first glance objects of the Carina arm are forming more open structure, but this impression is mainly based on the position of the complex 372 ($l = 311.2°$, $b = -0.4°$) (Russeil et al. 2007)(Fig. 8a). However, we can move it along the line of sight so that it falls exactly on the ring R_2 (for more details see section 5.4).

The mid-infrared observations show an excess of old stars in the direction of the Centaurus ($l \approx -50°$) and Scutum ($l \approx 25$–$31°$) arms but not in the direction of the Sagittarius arm ($l \approx +50°$) (Drimmel 2000; Churchwell et al. 2009). Sketch A can easily explain an increase of the density of old stars in the direction of the Centaurus arm (another name of the Crux arm). The line of sight in the direction of $l \approx -50$ is nearly tangent to the outer ring R_1 (Fig. 4). Observations and modelling show that the R_1 rings can be forming in the stellar subsystem, but the R_2 rings usually appear only in gas component (Byrd et al. 1994; Rautiainen & Salo 2000). However, we cannot explain the absence of an excess of old stars in the direction of the Sagittarius arm – in our model the Centaurus ($l \approx -50$) and Sagittarius ($l \approx +50$) arms are the segments of the same ring R_1 and, consequently, must have the same nature.

Distribution of optical objects in the Galactic plane also gives some evidences of the existence of a gap between the Sagittarius and Carina regions. Humphreys (1979) shows that OB-associations and young open clusters concentrate either in the Sagittarius region or in the Carina one but not in between. Recent studies based on the analysis of the distribution of young open clusters (Dias et al. 2002; Mermilliod & Paunzen 2003) and classical long-period Cepheids (Berdnikov et al. 2000) confirm the presence of the gap in the distribution of young objects along the Sagittarius-Carina arm (Majaess et al. 2009). This fact needs very accurate interpretation because spiral arms can have patchy structure. On the other hand, different kinematics of these regions suggests that they can belong to the different outer rings (Paper I).

Note that the inner ring in sketch B is larger and less elongated than that in sketch A (Fig. 8). Probably, this

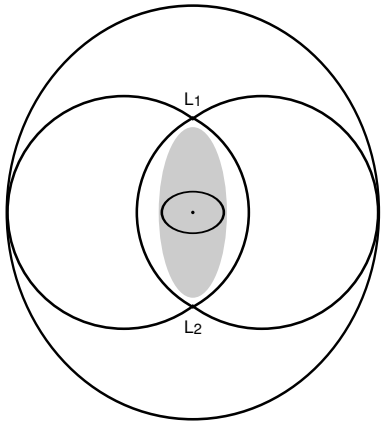

Figure 7. Basic model of the galactic ring structure. It includes the bar (gray ellipse), the nuclear ring which is represented by an ellipse aligned perpendicular to the bar, the inner ring elongated along the bar, the "8"-shaped outer ring R_1 stretched perpendicular to the bar, and the outer ring R_2 aligned with the bar.

larger ring can correspond to the case where the inner rings are forming farther away from the bar (Grouchy et al. 2010). Nevertheless, both types of the inner rings can be associated with the 3-kpc arm and its counterpart (Fux 1999; Dame & Thaddeus 2008; Rodriguez-Fernandez & Combes 2008).

At the moment we cannot say which conditions determine the exact place and shape of the inner ring-like structures and those of the outer rings R_1 in sketches A and B. In principle, the difference between them may be related to different kinds of orbits creating them: the very pointed inner ring in sketch A could be formed by the "classical" orbits that are found in barred potentials (Contopoulos & Grosbol 1989) whereas the rings/pseudorings in sketch B could be formed by manifold orbits (Athanassoula et al. 2010).

Our sketches also exhibit conspicuous differences in the shape and orientation of the nuclear gas condensation: in sketch A it is more round and elongated perpendicular to the bar while in sketch B it is oriented along the bar and looks like a secondary bar (Erwin 2011, and references therein). All our models have two ILR resonances located at distances $R_{ILR} = 0.2$ and 1.5 kpc (Papers I and II), so the difference between them cannot be caused by their position. Probably, it appears due to some features of the gas inflow. Special numerical simulations of the gas flow in the central region of the Galaxy show that 1-kpc nuclear ring can be holed and contain additional elliptical gas condensation with semi-axis of $a \approx 200$ and $b \approx 100$ pc which is associated with the Central Molecular Zone (CMZ) (Ferriére 2008; Rodriguez-Fernandez & Combes 2008), but our models have not enough resolution to reproduce this detail.

5.4 Kinematical distances

Most giant star-forming complexes have only kinematical distances which were calculated from the kinematical models with purely circular rotation law. Russeil (2003) reckons that photometrical distances for stars exciting HII regions are determined with the errors 20–30%. The errors in kinematical distances depend on the direction, but, on average, the deviations of the velocity V_{LSR} from the rotation curve of 15 km s^{-1} correspond to the error of $\sim 20\%$ in kinematical distances. However, this estimation was derived under the assumption that we always made a correct choice between the "far" and "near" distances on the same line of sight, but the non-circular gas motions significantly complicate this choice. In the case of wrong choice the distance error can exceed 100%.

We compared the observed V_{LSR} velocities of giant star forming complexes from the catalog by Russeil et al. (2007) with the model velocities of gas particles in model with analytical bar (Paper I). For each complex we selected model particles located within 200 pc from the observed position of a complex (l, r) and calculated their mean velocity along the line of sight. The mean difference between the model and observed V_{LSR} velocities is found to be $\Delta V = 16$ km s^{-1} which doesn't exceed significantly the mean difference between the observed V_{LSR} velocity and velocity calculated from the model rotation curve $\Delta V = 11$ km s^{-1}. Formally, the kinematical distances by Russeil et al. (2007) are quite reasonable.

The scale of kinematical distances is determined by the distance scale of objects used for calculation of rotation curve. If distances for objects studied and rotation curve are self-consistent then the velocity deviations from the rotation curve are always minimal and practically independent of the distance scale chosen.

Fig. 9 shows model V_{LSR} velocities calculated for different heliocentric distances r of the star-forming complex 372 ($l = 311.2°$, $b = -0.4°$) in the catalog by Russeil et al. (2007). We selected model particles (gas and OB) located within 200 pc from the chosen position of the complex and calculated their model V_{LSR} velocity. The number of model particles N within the 200-pc circle is also shown. The positions of the rings correspond to the maxima on curve $N(r)$. For each r we also determine the V_{LSR} velocity through the model rotation curve. We can see that complex 372 can be moved from the distance $r = 11.3$ to 10.2 kpc to fall exactly on the ring R_2, and its new position is in a good agreement with the observed V_{LSR}.

6 CONCLUSIONS

Model of the Galaxy with the outer ring R_1R_2' can explain some large-scale morphological features of the Galactic spiral structure. Ascending segments of the rings can be regarded as fragments of the trailing spiral arms while descending ones – as fragments of the leading arms. We found that the Carina arm falls well on the ascending segment of the ring R_2. Note also that the objects of the Sagittarius arm are located near the ascending segment of the ring R_1. The Carina-Sagittarius arm can consist of two ascending segments of the outer rings R_1 and R_2, which almost touch each other near the Carina region. It is possible that another pair of ascending segments of the outer rings can be identified with the Norma-Cygnus arm symmetrical to the Carina-Sagittarius one. The Perseus and Crux arms can be partially identified with the descending segments of the ring R_2. Thus, the two-component outer ring R_1R_2' can be mistakenly interpreted as the 4-armed spiral pattern.

Fourier analysis of the distribution of OB-associations

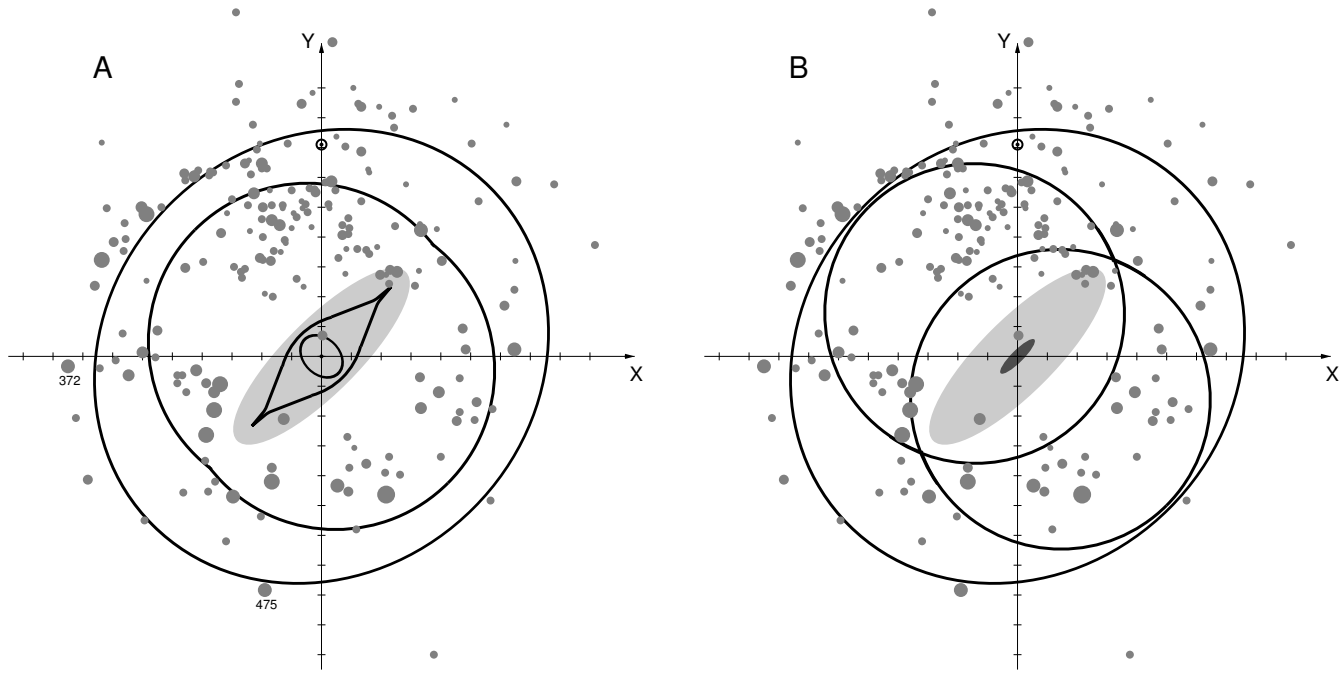

Figure 8. Ring structure applied to the Galaxy. In both sketches the bar is represented as a gray ellipse with the semi-axes $a = 4.0$ and $b = 1.2$ kpc. The position angle of the Sun with respect to the bar is $\theta_b = 45°$. The outer ring R_2 is shown by an ellipse elongated along the bar with the semi-axes $a_2 = 8.0$ and $b_2 = 7.2$ kpc. Sketch A is determined by the distribution of particles in model with analytical bar (Paper I) while sketch B is based on the distribution of particles in N-body simulations (Paper II). We can see a gap between two outer rings R_1 and R_2 in sketch A but it is absent in sketch B. Sketch A has the more elongated and smaller inner ring in comparison with that in sketch B. There are also some differences in the shape and orientation of the nuclear gas condensation in sketches A and B. Also shown the distribution of giant star-forming complexes ($U > 60$ pc cm^{-2}) (Russeil et al. 2007). The value of R_0 is adopted to be $R_0 = 7.1$ kpc

with the same kinematic characteristics over spiral harmonics shows the presence of a leading component in the spiral structure of the Galaxy (Mel'nik 2005). The sample includes OB-associations whose radial component V_R of velocity is directed toward the Galactic center. The appearance of the leading spiral agrees with the position of the Sun near the descending segment of the ring R_2, which can be thought as a fragment of the leading spiral arm.

Model of the two-component outer ring could also explain the existence of some tangential directions corresponding to the emission maxima near the terminal velocity curves. Model diagrams (l, V_{LSR}) reproduce the maxima in the direction of the Carina, Crux, Norma, and Sagittarius arms. Additionally, N-body model yields the maxima in the directions of the Scutum and 3-kpc arms.

On the basis of numerical simulations we propose two sketches of the ring structure of the Galaxy which includes the bar, two outer rings, the inner ring, and the nuclear gas condensation forming the nuclear ring and/or the secondary bar (Fig. 8ab). Both sketches can explain the position of the Carina-Sagittarius arm with respect to the Sun. Sketch A can also explain the existence of an excess of old stars in the direction of the Centaurus arm $l \approx -50$.

ACKNOWLEDGMENTS

We wish to thank Heikki Salo for using his simulation code. We are grateful to N.Ya. Sotnikova and P. Grosbol for useful remarks and interesting discussion. This work was partly supported by the Russian Foundation for Basic Research (project nos. 10-02-00489).

REFERENCES

Adler D. S., Roberts W. W., 1992, ApJ, 384, 95
Anderson L. D., Bania T. M., 2009, ApJ, 690, 706
Athanassoula E., 1984, Phys. Rep., 114, 321
Athanassoula E., 1992, MNRAS, 259, 328
Athanassoula E., Romero-Gómez M., Bosma A., Masdemont J. J., 2010, MNRAS, 407, 1433
Babusiaux C., Gilmore G., 2005, MNRAS, 358, 1309
Benjamin R. A., Churchwell E., Babler B. L., Indebetouw R., Meade M. R., Whitney B. A., Watson C., Wolfire M. G. et al., 2005, ApJ, 630, L149
Berdnikov L. N., Dambis A. K., Vozyakova O. V., 2000, A&AS, 143, 211
Bertin G., Lin C.C., 1996, Spiral Structure in Galaxies: A Density Wave Theory, Cambridge, MA: MIT Press
Binney J., Gerhard O., Stark A. A., Bally J., Uchida K. I., 1991, MNRAS, 252, 210
Binney J., Tremaine S., 2008, Galactic Dynamics, 2-nd edn. Princeton, NJ, Princeton Univ. Press
Bissantz N., Englmaier P., Gerhard O., 2003 MNRAS, 340, 949
Bissantz N., Gerhard O., 2002 MNRAS, 330, 591
Blaha C., Humphreys R. M., 1989, AJ, 98, 1598

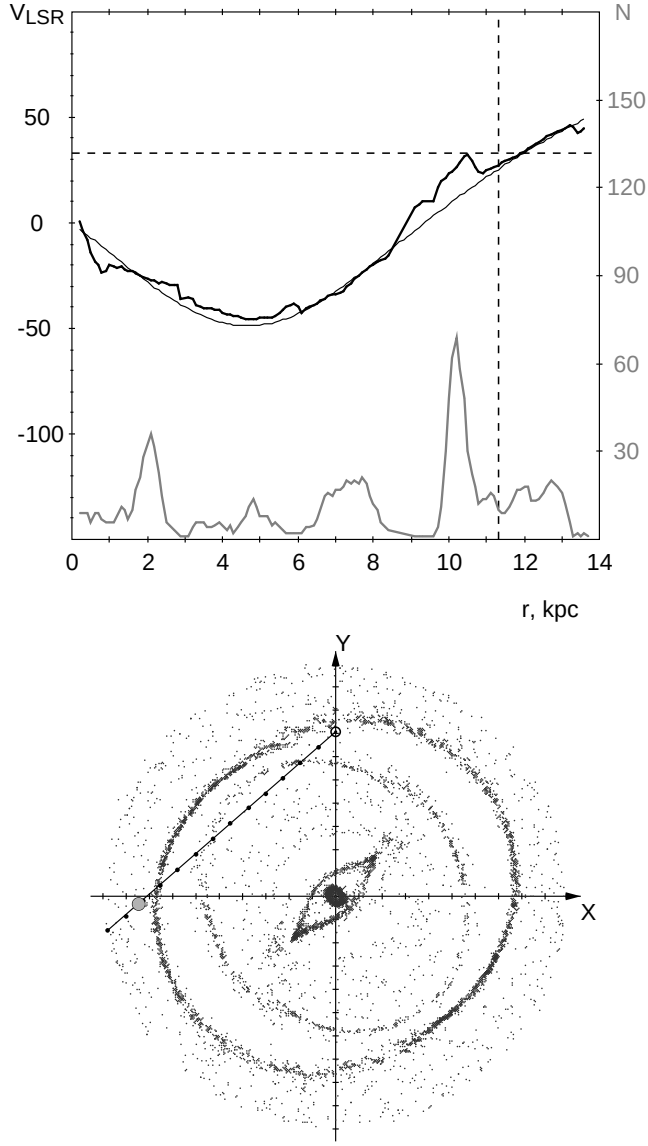

Figure 9. *Upper plot*: Model V_{LSR} velocities (black thick line) calculated for different heliocentric distances r of the star-forming complex 372 ($l = 311.2°, b = -0.4°$) (Russeil et al. 2007). Dashed lines indicate the observed V_{LSR} velocity ($V_{LSR} = 33.0$ km s^{-1}) and the catalog value of the kinematical distance reduced to the short distance scale ($r = 11.3$ kpc). Gray line indicates the number of particles N within the 200-pc circle at the chosen r. Left vertical axis (black one) shows the scale for V_{LSR} velocities while the right axis (gray one) exhibits the scale for N. Thin black line indicates V_{LSR} calculated through the model rotation curve. *Lower plot*: the position of the complex 372 in the galactic plane with respect to the distribution of model particles (Paper I). The line of sight with 1-kpc divisions is also shown.

Blitz L., Binney J., Lo K. J., Bally J., Ho P. T. P., 1993, Nature, 361, 417

Blitz L., Spergel D. N., 1991, ApJ, 379, 631

Burton W. B., Bania T. M., 1974, A&A, 33, 425

Burton W. B., Shane W. W., 1970, in Becker W., Contopoulos G. I., eds, Proc. IAU Symp. 38, The Spiral Structure of our Galaxy. Dordrecht, Reidel, p. 397.

Buta R., 1986, ApJS, 61, 609

Buta R., 1995, ApJS, 96, 39

Buta R., Combes F., 1996, Fund. Cosmic Physics, 17, 95

Buta R., Corwin H. G., Odewahn S. C., 2007, The de Vaucouleurs Atlas of Galaxies. Cambridge, NY, Cambridge Univ. Press

Buta R., Crocker D. A., 1991, AJ, 102, 1715

Byrd G., Rautiainen P., Salo H., Buta R., Crocker D. A., 1994, AJ, 108, 476

Cabrera-Lavers A., Hammersley P. L., González-Fernández C., López-Corredoira M., Garzón F., Mahoney T. J., 2007, A&A, 465, 825

Caswell J. L., Haynes R. F., 1987, A&A, 171, 261

Chakrabarty D., 2007, A&A, 467, 145

Churchwell E., Babler B. L., Meade M. R., Whitney B. A., Benjamin R. et al., 2009, PASP, 121, 213

Cohen R. S., Dame T. M., Thaddeus P., 1986, ApJS, 60, 695

Contopoulos G., Grosbol P., 1989, A&AR, 1, 261

Contopoulos G., Papayannopoulos Th., 1980, A&A, 92, 33

Dambis A. K., Mel'nik A. M., Rastorguev A. S., 1995, Astron. Lett., 21, 291

Dambis, A. K., Mel'nik, A. M., Rastorguev, A. S., 2001, Astron. Lett., 27, 58

Dame T. M., Elmegreen B. G., Cohen R. S., Thaddeus P., 1986, ApJ, 305, 892

Dame T. M., Hartmann D., Thaddeus P., 2001, ApJ, 547, 792

Dame T. M., Thaddeus P., 2008, ApJ, 683, L143

Dehnen, W. 2000, AJ, 119, 800

Dias W. S., Alessi B. S., Moitinho A., Lepine J. R. D., 2002, A&A, 389, 871

Downes D., Wilson T. L., Bieging J., Wink J., 1980 A&AS, 40, 379

Drimmel R., 2000, A&A, 358, L13

Efremov Yu. N., 1998, Astron. Astrophys. Trans., 15, 3

Efremov Yu. N., 2011, Astron. Rep., 55, 108

Englmaier P., Gerhard O., 1999, MNRAS, 304, 512

Englmaier P., Gerhard O., 2006, CeMDA, 94, 369

Erwin P., 2011, Mem. S. A. It. Suppl., 18, 145

Ferriére K., 2008, AN, 329, 992

Fux R., 1999, A&A, 345, 787

Fux R., 2001, A&A, 373, 511

Georgelin Y. M., Georgelin Y. P., 1976, A&A, 49, 57

Gerhard O., 2011, Mem. S. A. It. Suppl., 18, 185

Glushkova E. V., Dambis A. K., Mel'nik A. M., Rastorguev A. S., 1998, A&A, 329, 514

Grabelsky D. A., Cohen R. S., Bronfman L., Thaddeus P., 1988, ApJ, 331, 181

Grouchy R. D., Buta R. J., Salo H., Laurikainen E., 2010, ApJ, 139, 2465

Habing H. J., Sevenster M. N., Messineo M., van de Ven G., Kuijken K., 2006, A&A, 458, 151

Henderson A. P., Jackson P. D., Kerr F. J., 1982, ApJ, 263, 116

Hou L. G., Han J. L., Shi W. B., 2009, A&A, 499, 473

Humphreys R. M., 1976, ApJ, 206, 114

Humphreys R. M., 1979 in Burton W. B., ed, Proc. IAU Symp. 84, The Large-Scale Characteristics of the Galaxy. Dordrecht, Reidel, p. 93.

Humphreys R. M, McElroy D. B., 1984, ApJ, 284, 565

Kalberla P. M. W., Berton W. B., Hartmann D., Arnal

E. M., Bajaja E., Morras R., Pöppel W. G. L., 2005, A&A, 440, 775
Kalnajs A. J., 1973, Proc. ASA, 2, 174
Kalnajs A. J., 1991, in Sundelius B., ed., Dynamics of Disc Galaxies. Göteborgs Univ., Göthenburg, p. 323
Kerr F. J., 1962, MNRAS, 123, 327
Kerr F. J., 1970, in Becker W., Contopoulos G. I., eds, Proc. IAU Symp. 38, The Spiral Structure of our Galaxy. Dordrecht, Reidel, p. 95
Levine E. S., Blitz L., Heiles C., 2006, Sci, 312, 1773
Lin C. C., Shu F. H., 1964, ApJ, 140, 646
Lin C. C., Yuan C., Shu F. H., 1969, ApJ, 155, 721
Lockman F. J., 1979, ApJ, 232, 761
Majaess D. J., Turner D. G., Lane D. J., 2009, MNRAS, 398, 263
Masset F., Tagger M., 1997, A&A, 322, 442
Mihalas D., Binney J., 1981, Galactic Astronomy, 2-nd edn. San Francisco, CA, W. H. Freeman and Co.
Minchev I., Boily C., Siebert A., Bienayme O., 2010, MNRAS, 407, 2122
Mel'nik A. M., 2003, Astron. Lett., 29, 304
Mel'nik A. M., 2005, Astron. Lett., 31, 80
Mel'nik A. M., 2006, Astron. Lett., 32, 7
Mel'nik A. M., Dambis A. K., 2009, MNRAS, 400, 518
Mel'nik A. M., Dambis A. K., Rastorguev A. S., 1999, Astron. Lett., 25, 518
Mel'nik A. M., Dambis A. K., Rastorguev A. S., 2001, Astron. Lett., 27, 521
Mel'nik A. M., Rautiainen P., 2009, Astron. Lett., 35, 609 (Paper I)
Mermilliod J.-C., Paunzen E., 2003, A&A, 410, 511
Oort J. H., Kerr F. J., Westerhout G., 1958, MNRAS, 118, 379
Paladini R., Davies R. D., DeZotti G., 2004, MNRAS, 347, 237
Pohl M., Englmaier P., Bissantz N., 2008 ApJ, 677, 283
Rastorguev A. S., Pavlovskaya E. D., Durlevich O. V., Filippova A. A., 1994, Astron. Lett., 20, 591
Rautiainen P., Mel'nik A. M., 2010, A&A, 519, 70 (Paper II)
Rautiainen P., Salo H., 1999, A&A, 348, 737
Rautiainen P., Salo H., 2000, A&A, 362, 465
Roberts W. W., 1972, ApJ, 173, 259
Rodriguez-Fernandez N. J., Combes F., 2008, A&A, 489, 115
Russeil D., 2003, A&A, 397, 133
Russeil D., Adami C., Georgelin Y. M., 2007, A&A, 470, 161
Salo H., 1991, A&A, 243, 118
Salo H., Laurikainen E., 2000, MNRAS, 319, 377
Schwarz M. P., 1981, ApJ, 247, 77
Sellwood J. A., 2000, Ap&SS, 272, 31
Sellwood J. A., 2011, MNRAS, 410, 1637
Sellwood J. A., Kahn F. D., 1991, MNRAS, 250, 278
Sellwood J. A., Lin D. N. C., 1989, MNRAS, 240, 991
Sellwood J. A., Sparke L. S., 1988, MNRAS, 231, 25
Simonson S. C. 1970, A&A, 9, 163
Sitnik T. G., 2003, Astron. Lett., 29, 311
Sitnik T. G., Mel'nik A. M., 1996, Astron. Lett., 22, 422
Toomre A., 1977, ARA&A, 15, 437
Vallée J. P., 2005, AJ, 130, 569
Vallée J. P., 2008, AJ, 135, 1301
Watson C., Araya E., Sewilo M., Churchwell E., Hofner P., Kurtz S., 2003, AJ, 587, 714
Weiner B. J., Sellwood J. A., 1999, ApJ. 524, 112